European Journal of Radiology Open 10 (2023) 100492

Contents lists available at ScienceDirect

European Journal of Radiology Open

journal homepage: www.elsevier.com/locate/ejro

Opportunistic AI-enabled automated bone mineral density measurements in lung cancer screening and coronary calcium scoring CT scans are equivalent

Morteza Naghavi [a,*], Isabel De Oliveira [a], Song Shou Mao [b], Amirhossein Jaberzadeh [a], Juan Montoya [a], Chenyu Zhang [a], Kyle Atlas [a], Venkat Manubolu [b], Marlon Montes [a], Dong Li [c], Thomas Atlas [a], Anthony Reeves [e], Claudia Henschke [d], David Yankelevitz [d], Matthew Budoff [b]

[a] HeartLung AI Technologies, TMC Innovation, 2450 Holcomb Blvd, Houston, TX 77021
[b] Lundquist Institute, Harbor UCLA Medical Center, 1124 W Carson St, Torrance, CA 90502, USA
[c] Emory University, 201 Dowman Dr, Atlanta, GA 30322, USA
[d] Mount Sinai, 1176 5th Ave, MC Level, New York, NY 10029, USA
[e] Cornell University, Ithaca, NY 14850, USA

ARTICLE INFO

Keywords:
Bone mineral density
Artificial intelligence
Deep learning
Opportunistic
Coronary artery calcium score
Quantitative computed tomography
Osteoporosis
Osteopenia
Cardiovascular Screening
Lung cancer screening

ABSTRACT

Rationale and objectives: We previously reported a novel manual method for measuring bone mineral density (BMD) in coronary artery calcium (CAC) scans and validated our method against Dual X-Ray Absorptiometry (DEXA). Furthermore, we have developed and validated an artificial intelligence (AI) based automated BMD (AutoBMD) measurement as an opportunistic add-on to CAC scans that recently received FDA approval. In this report, we present evidence of equivalency between AutoBMD measurements in cardiac vs lung CT scans.
Materials and methods: AI models were trained using 132 cases with 7649 (3 mm) slices for CAC, and 37 cases with 21918 (0.5 mm) slices for lung scans. To validate AutoBMD against manual measurements, we used 6776 cases of BMD measured manually on CAC scans in the Multi-Ethnic Study of Atherosclerosis (MESA). We then used 165 additional cases from Harbor UCLA Lundquist Institute to compare AutoBMD in patients who underwent both cardiac and lung scans on the same day.
Results: Mean±SD for age was 69 ± 9.4 years with 52.4% male. AutoBMD in lung and cardiac scans, and manual BMD in cardiac scans were 153.7 ± 43.9, 155.1 ± 44.4, and 163.6 ± 45.3 g/cm^3, respectively ($p = 0.09$). Bland-Altman agreement analysis between AutoBMD lung and cardiac scans resulted in 1.37 g/cm^3 mean differences. Pearson correlation coefficient between lung and cardiac AutoBMD was $R^2 = 0.95$ ($p < 0.0001$).
Conclusion: Opportunistic BMD measurement using AutoBMD in CAC and lung cancer screening scans is promising and yields similar results. No extra radiation plus the high prevalence of asymptomatic osteoporosis makes AutoBMD an ideal screening tool for osteopenia and osteoporosis in CT scans done for other reasons.

1. Introduction

Global deaths, and DALYs (disability-adjusted life-years) attributable to low bone mineral density (BMD) increased from 207,367 and 8588,936 in 1990 to 437,884 and 16,647,466 in 2019, an increase of 111.16% and 93.82%, respectively [1]. More than 10 million Americans over the age of 50 are currently affected by osteoporosis and another 44 million have low BMD, also known as osteopenia [2]. Osteoporotic individuals are usually asymptomatic and unaware of their condition prior to experiencing a fracture, therefore screening for osteoporosis is recommended by US Preventive Services Task Force [3]. With appropriate treatment, about half of all osteoporosis-related repeat fractures can be prevented [4]. The only way to identify these individuals prior to the occurrence of a fracture and apply appropriate treatment to prevent further bone loss is through a BMD screening test [5].

Dual-energy x-ray absorptiometry (DEXA) is the current clinical imaging standard for assessing BMD [5]. However, only one out of five people who should get a DEXA scan actually get one [6]. Additionally,

* Corresponding author.
E-mail address: mn@vp.org (M. Naghavi).

https://doi.org/10.1016/j.ejro.2023.100492

DEXA is limited by its 2D planar technique [7] and therefore unable to distinguish cortical from trabecular bone so that it averages both cortical and trabecular bone tissues for BMD measurement. However, cortical bone tissues often have degenerative calcifications such as osteophytes, which erroneously exaggerate BMD scores in DEXA. As a result, numerous studies have shown that DEXA overestimates BMD in certain groups, particularly in the obese population, which is on the rise in the US [8–11]. DEXA is prone to under-detecting patients who are suffering from osteoporosis, which perpetuates the problem of this condition being both underdiagnosed and undertreated. This, in turn, leads to high morbidity and mortality rates associated with osteoporosis [12].

Quantitative Computed Tomography (QCT) using QCT-BMD Analysis Software (Image Analysis, Inc) on low dose cardiac and thoracic CT images was introduced over a decade ago [10–13]. Compared to DEXA, QCT is a more sensitive method for measuring BMD [12,14–16] and has three unique advantages: 1) the ability to clearly separate cortical and trabecular bone tissues; 2) the ability to offer real volumetric density in units of mg/cc; 3) high-resolution three-dimensional images of bone morphometry [13]. The ability to separate trabecular and cortical bone tissues with QCT allows for exclusively averaging trabecular bone tissue for BMD measurement and therefore avoiding underestimation of bone loss due to measurements made on cortical bone tissue.

Coronary Artery Disease (CAD) is a leading cause of mortality worldwide. Early detection of asymptomatic CAD is crucial because in over half of CAD victims the first symptom is sudden cardiac death [17]. The addition of Coronary Artery Calcium (CAC) score to the latest guidelines issued jointly by the American College of Cardiology and American Heart Association has sparked growing interest in the use of cardiac CT scans for obtaining CAC scores to predict and prevent adverse CAD events [18].

Lung cancer is the second most common cancer in the United States, and accounts for the greatest number of cancer deaths in both men and women worldwide [19]. Early detection of lung cancer has been challenging and it was not until 2011 with the release of data from the National Lung Cancer Screening Trial (NLST) that a screening test for lung cancer was demonstrated to reduce lung-cancer specific mortality [20]. This trial demonstrated that using low dose computed tomography (LDCT) for lung cancer screening resulted in a significant reduction in lung cancer mortality [21]. LDCT has become the standard of care for lung cancer screening ever since.

1.1. AI-enabled opportunistic add-on BMD measurements

Cardiac and lung CT scans are obtained each year in large quantities for CAD prediction and lung cancer screening. Using the images from these scans for opportunistic BMD reporting presents a great opportunity for early detection of osteopenia and osteoporosis.

Medical imaging is among the most promising clinical applications of artificial intelligence (AI), and mounting attention is being directed towards establishing and fine-tuning its performance to facilitate the detection and quantification of various pathologies [22]. Numerous FDA approvals are obtained each year for various clinical indications using AI as a decision support tool.

Training AI to rapidly detect various abnormalities in a single lung and cardiac CT scan makes logical sense since these scans encompass multiple organs. In the case of BMD, this added value is even more significant considering that manual measurements of BMD using QCT technique is time consuming and has potential for human error.

Leveraging a CT-based assessment of vertebral trabecular bone density for BMD measurement presents a great opportunity which our group has taken from the idea stage to FDA approval. The purpose of this study is to show that AutoBMD is capable of measuring BMD from both lung and cardiac CT scans with an accuracy level comparable to manual measurements. Additionally, this study aims to demonstrate that for the same patient, there are comparable results obtained from cardiac and lung CT scans.

2. Methods

2.1. Study population

We used 165 cases from Harbor UCLA Lundquist Institute who underwent both cardiac and lung CT scans on the same day, and 6776 CAC scans from MESA to validate this against manual measurements. MESA is considered the largest multi-ethnic study of atherosclerotic cardiovascular disease in the world and was chosen because it has the largest number of manual measurements of BMD using quantitative CT. Budoff et al. first reported manual BMD measurements in various MESA studies 10–12, 23–28. Both cardiac and lung CT scanning techniques were conducted according to MESA protocol. The reconstruction thicknesses were 2.5 mm and 0.5 mm for cardiac and lung scans, respectively. Detailed operating manual of CT scan methods and protocols are publicly available at MESA website [29].

2.2. Manual BMD measurements

The ground truth BMD values for the MESA dataset were obtained from manual BMD measurements done by trained operators using QCT-BMD Analysis Software (Image Analysis, Inc). Measurements were obtained from three consecutive thoracic vertebrae starting at the level that contained the left main coronary artery caudally [10,11]. The region of interest was centered in the trabecular portion of the vertebral bodies, 2–3 mm in from the cortical surface. The segmentations were used to calculate the mean Hounsfield units, a standardized CT coefficient, and subsequently the BMD value. The mean BMD for the three consecutive vertebral bodies was calculated in all subjects [10,11].

2.3. Auto-BMD AI model

Automation of BMD measurements requires the identification of individual vertebrae, the location of the intervertebral discs, and the subsequent removal of the cortical bone layer. Two Deep Learning models were developed for cardiac and full chest CT scan images comprising of 7649 and 21,918 slices, respectively. The models were trained to identify trabecular bone and disks with a training data set of 132 cardiac and 37 lung CT images. Table 1.

Ground Truth labeling for the vertebral bones was performed by three trained technicians and overseen by a radiologist. Software segmentation validation criteria for vertebral bones was set as a Dice coefficient of 0.95 for cardiac and 0.97 for lung CT scans. Further training of the software was ceased upon reaching the predefined Dice Score. Fig. 1.

To validate AutoBMD across both cardiac and lung scans against manual measurements as the Ground Truth, we used only one set of reference comprising 991 cases of BMD measured manually on CAC scans in MESA. Each deep learning model has two steps to automatically detect individual vertebrae and disks. In the first step, the model was trained to focus on the whole spine area. Transfer learning was then used to train for disk locations using the pretrained model. The architecture of the model consists of an encoder and a decoder. The encoder is a UNet with 12 layers of 2D convolutions, skip connections, Leaky ReLu activations and batch normalization. The decoder is a 3-layer convolution 2D with Leaky ReLu activations and a sigmoid at the end. Signal processing was used to erode the borders to segment the entire vertebral bone. Fig. 2.

2.4. AutoBMD in lung and cardiac CT scans

The AI models were used on lung and cardiac CT scans from the 165 cases who underwent these scans on the same day. Manual BMD measurements in MESA cardiac scans were compared to AutoBMD measurements from both cardiac and lung CT scans.

An example of manual BMD vs AutoBMD measurements for both

Table 1
Training and Validation data.

Image protocol	Training images (70%)	Training slices	Training Vertebrae	Validation images (30%)	Validation slices	Validation vertebrae
Thick slice 2.5 mm (cardiac)	132	7649	895	56	3241	380
Thin slice 0.5 mm (full chest/ Lung)	37	21,918	444	16	9393	192

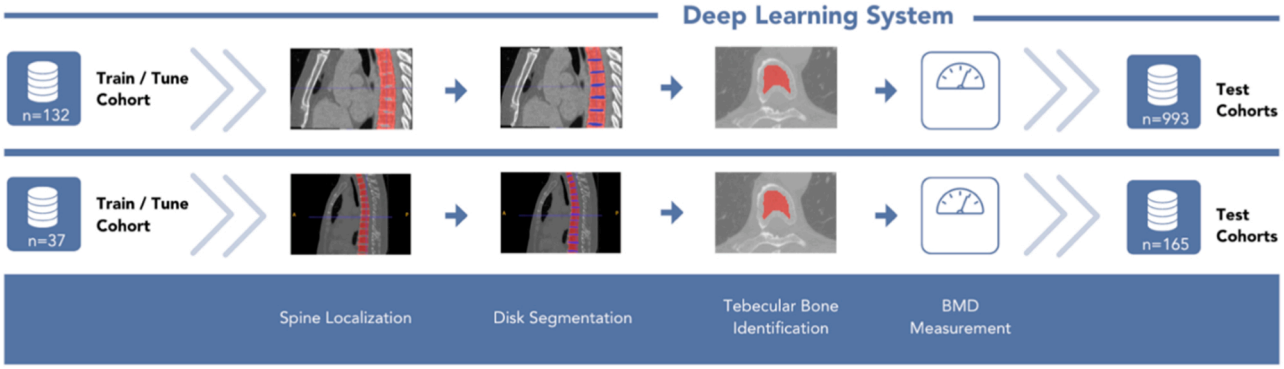

Fig. 1. Deep learning system of the Auto-BMD Software, including spine localization, disk segmentation, trabecular bone identification and BMD measurement. Software developed for cardiac CT scans is shown by the top flowchart and software developed for lung CT scans by the bottom flowchart.

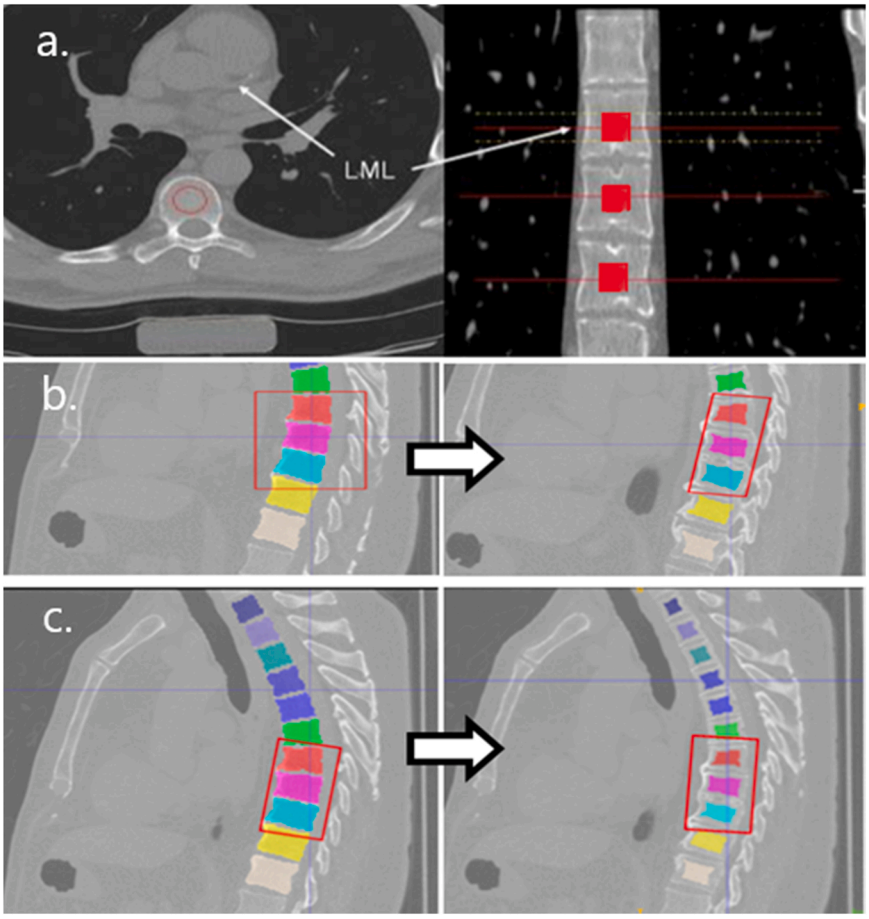

Fig. 2. a. Manual BMD measurement on cardiac CT scan is outlined by 10 mm circle on axial image (left) and indicated by horizontal lines on sagittal image (right). 10 mm rods are inserted in the middle of the trabecular vertebral bones, depicted as red cylinders in the right image. Measurement started at level of the section containing left main coronary artery caudally. **b.** AutoBMD measurement on CAC CT scan. The left image shows segmentations for the full vertebral body and the right image shows segmentations of the trabecular component of the vertebral body. BMD is measured in the trabecular bone in the center of each vertebra. Circled vertebrae are correlated to the circled vertebrae on Fig. 2c. **c.** AutoBMD measurement on lung CT scan. The left image shows segmentations for the full vertebral body and the right image shows segmentations of the trabecular component of the vertebral body. BMD is measured in the trabecular bone in the center of each vertebra. Circled vertebrae are correlated to the circled vertebrae on Fig. 2b.

cardiac and lung CT scans is shown below.

All tests of significance were two tailed, and significance was defined at the $P < 0.05$ level. Separate ANOVA tests for the decline in BMD averages from T1 to T12 in lung scans and T6 to T11 in cardiac scans were also performed.

3. Results

All values are reported as means ± SD. Mean±SD for age was 69 ± 9.4 years with 52.4% male. AutoBMD in lung and cardiac scans, and manual BMD in cardiac scans were 153.7 ± 43.9 g/cm^3, 155.1

± 44.4 g/cm^3, and 166.3 ± 47.9 g/cm^3, respectively (p = 0.09) (Fig. 3).

Average BMD declined from T1 to T12 in lung CT scans and T6 to T11 in cardiac CT scans. Average BMD measured in lung CT scans were as following: T1: 202.6 ± 53.0 g/cm^3, T2: 191.6 ± 49.8 g/cm^3, T3: 180.5 ± 49.4 g/cm^3, T4: 171.6 ± 48.5 g/cm^3, T5: 165.0 ± 46.5 g/cm^3, T6: 160.7 ± 48.4 g/cm^3, T7: 156.3 ± 44.6 g/cm^3, T8: 152.8 ± 45.8 g/cm^3, T9: 152.2 ± 44.9 g/cm^3, T10: 153.3 ± 43.4 g/cm^3, T11: 146.0 ± 44.0 g/cm^3 and T12: 130.8 ± 40.1 g/cm^3 (Fig. 4a). Average BMD measured in cardiac CT scans were as follows: T6: 162.1 ± 47.9 g/cm^3, T7: 152.1 ± 47.2 g/cm^3, T8: 154.0 ± 44.1 g/cm^3, T9: 154.5 ± 46.3 g/cm^3, T10: 152.7 ± 54.0 g/cm^3 and T11: 143.5 ± 65.6 g/cm^3 (Fig. 4b). + .

AutoBMD on average detected 4.4 vertebral bodies in cardiac CT scans and 12.3 in lung CT scans. AutoBMD detected the first vertebral body in lung scans as T1. Generally vertebral bodies 2–4 in cardiac scans corresponded to T7 to T9 in lung scans. Therefore, AutoBMD used T7 to T9 in lung scans and vertebrae 2–4 in cardiac scans. As a result, for consistency and standardizing the measurements, we chose to compare vertebra 2–4 on cardiac scans with T7 to T9 in lung scans. Average AutoBMD obtained for T7 to T9 was 153.7 ± 43.9 g/cm^3 in lung scans and 155.1 ± 44.4 g/cm^3 in cardiac scans. A strong correlation (R^2 =0.95) was found between the AutoBMD obtained for these corresponding vertebral bodies between cardiac and lung scans (Fig. 5) and Bland-Altman agreement analysis for these corresponding vertebral bodies resulted in 1.37 g/cm^3 mean differences (Fig. 6).

4. Discussion

We have previously reported manual and AI-enabled automated opportunistic BMD measurements in cardiac CT scans obtained for CAC score [10–12,23–37]. In this study we have demonstrated the equivalency of automated BMD measurements in cardiac CT scans obtained for CAC scoring vs chest CT scans for lung cancer screening. Furthermore, our study presents a compelling opportunity to leverage CAC and lung cancer screening CT scans for early detection and treatment of osteopenia and osteoporosis without subjecting patients to additional radiation, additional DEXA scans, or excessive costs.

Approximately 20 million cardiac and lung CT scans are performed every year on the United States and many more worldwide [30]. The economic value of AI-enabled opportunistic use of these scans for BMD screening is enormous. Although manual measurement of BMD is feasible as we have reported in the past [10–13, 24, 26], it relies on skilled worker time, attention to details, and consistency, all of which can be obviated with AI [31]. Furthermore, it is not feasible to avoid hypercalcified pixels (HU>400) when carrying out manual measurements, which may result in overestimation of BMD.

This study shows that an AI-based tool can provide opportunistic BMD measurements both in lung and cardiac CT scans. A similar approach could be taken for measuring BMD using existing CT scans within each hospital's PACS (picture archiving and communication system). In the United States, payers may cover measurements done on CT scans done within 12 months of the BMD measurement. Although the variability of scanners and related coefficient of calibration must be addressed, this opportunistic approach to osteoporosis screening is promising and can lead to early detection and treatment of at-risk individuals. Some of these patients may undergo subsequent DEXA scans for prospective monitoring. Alerting individuals that have a below average BMD for their age can raise awareness of bone health. It can also be used to encourage patients to adopt lifestyle modifications or take appropriate medications to prevent a future fracture. One advantage of the opportunistic AutoBMD approach is no extra radiation to patients. Even though DEXA scans impose significantly less radiation than CT scans, AutoBMD imposes zero radiation by nature.

Beyond imaging, the use of AI for population bone health has been reported by Chiu et al. [32] who developed an artificial neural network attuned to 7 predictive demographic and lifestyle variable.

for the prediction of osteoporosis, with a sensitivity of 78.3% and specificity of 73.3%. Their findings contribute to the work of several others, all of which help to demonstrate the efficacy of AI in predicting osteoporotic disease [33,34]. Cohen et al. reported opportunistic BMD measurements using PET-CT in Hodgkin lymphoma patients undergoing chemotherapies [35]. They have demonstrated a significant decline in BMD after vs before chemotherapy. Opportunistic use of PET-CT scan has the potential to detect Hodgkin lymphoma patients at high risk for developing osteoporosis and to guide clinicians regarding monitoring and intervention [35].

Limitations of this study include previously obtained manual BMD measurements from CT scans in MESA some 10–20 years ago which may not represent CT scans of today and the next 10–20 years. We would need to calculate calibration coefficient for new CT scanners. However, this is a rather insignificant problem and can be recalibrated within 30 min for each scanner.

The decline in BMD from T1 to T12 seen in our study corroborates earlier reports [36,37] and necessitates the use of specific vertebral bodies (e.g., T7-T9) for measuring and monitoring changes in BMD.

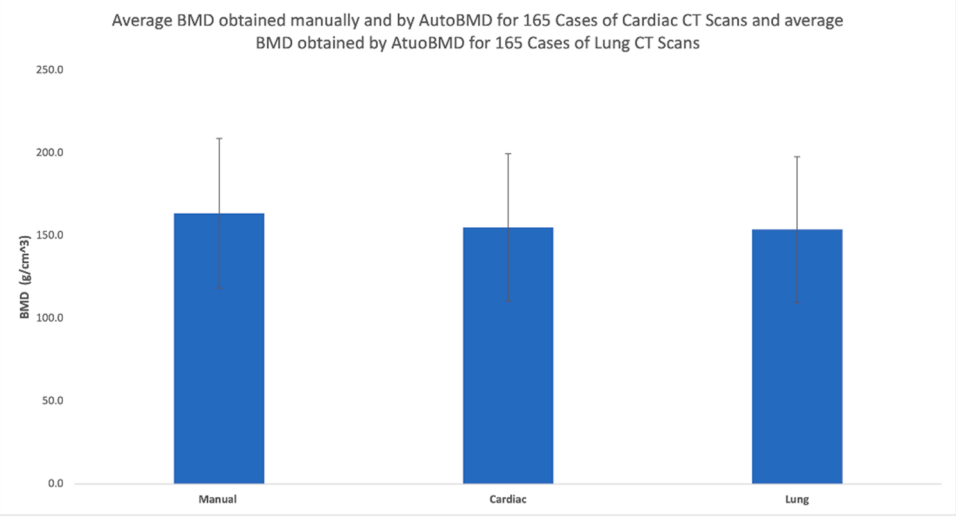

Fig. 3. Average BMD obtained from both manual and AutoBMD for 165 Cardiac CT cases and average BMD obtained from AutoBMD for corresponding 165 lung CT cases (p = 0.09).

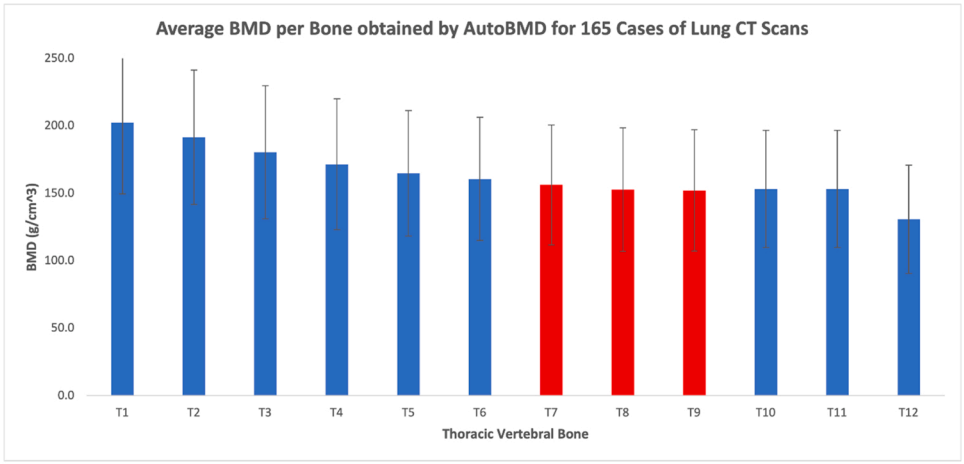

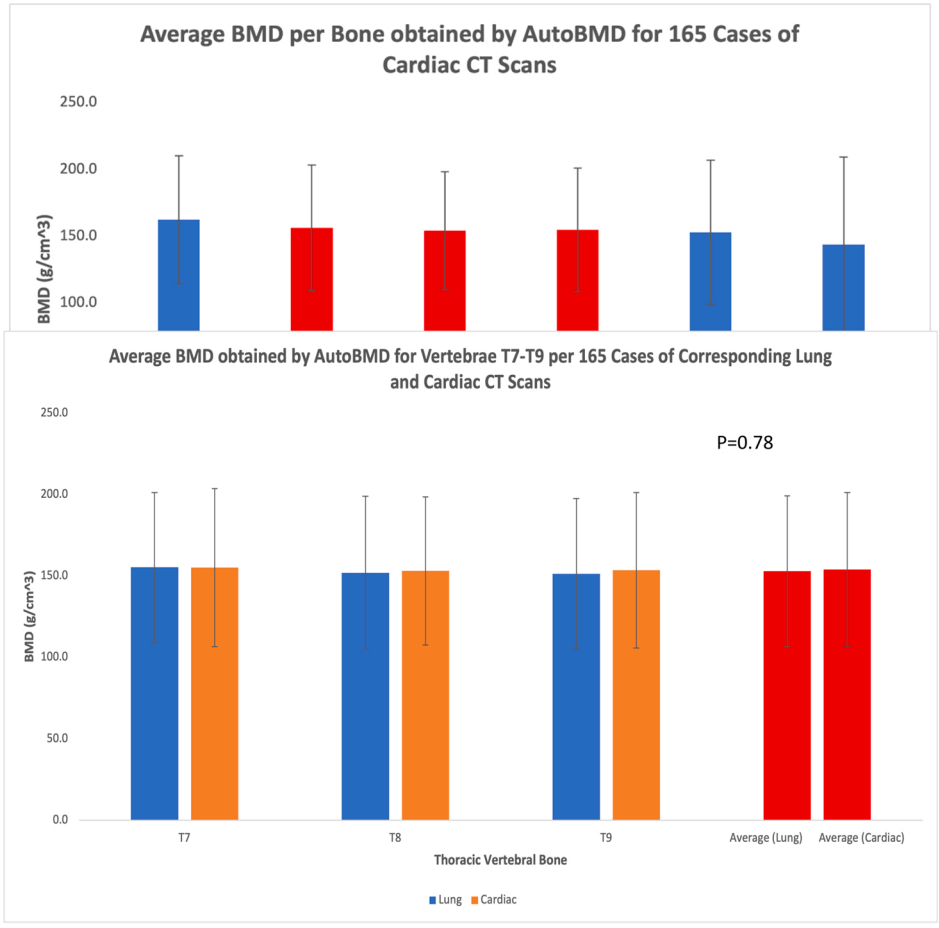

Fig. 4. a. AutoBMD results obtained for the average BMD per vertebra (T1 to T12) in 165 lung CT scans. n = 165 for T1 to T10, n = 160 for T11 and n = 138 for T12. b. AutoBMD results obtained for the average BMD per vertebra in 165 cardiac scans. n = 165 for T6 to T8, n = 140 for T9, n = 60 for T10 and n = 8 for T11. Highlighted columns represent vertebrae that showed a strong correlation with vertebrae represented by highlighted columns on Fig. 4a. c. AutoBMD results obtained for the average BMD for vertebrae T7 to T9 in 165 corresponding lung and cardiac CT scans. For all vertebrae, n = 165, with the exception of T9 for cardiac for which n = 150.

Therefore, a potential limitation of AutoBMD is that the number of vertebrae captured by AutoBMD in cardiac and lung CT scans depends on the field of view, which varies between patients. If any of these vertebrae are fractured or hindered by artifacts the AutoBMD measurements could be affected. This limitation is remedied by flagging such cases and bringing them to the attention of reporting radiologists. An important consideration must be given to monitoring BMD changes in cases with multiple CT scans overtime. To our knowledge a thorough investigation on this topic is missing and our group is currently conducting relevant studies to demonstrate the value of opportunistic AutoBMD monitoring over time.

5. Conclusion

Opportunistic screening for subclinical low-BMD in CT scans done for cardiac and lung cancer screening is feasible and comparable. Given that such an approach saves patients extra radiation and cost, it warrants further investigations. If corroborated in other studies, healthcare providers must consider the potential of AutoBMD to improve patient care in a cost-effective manner.

Ethical

None/Not applicable.

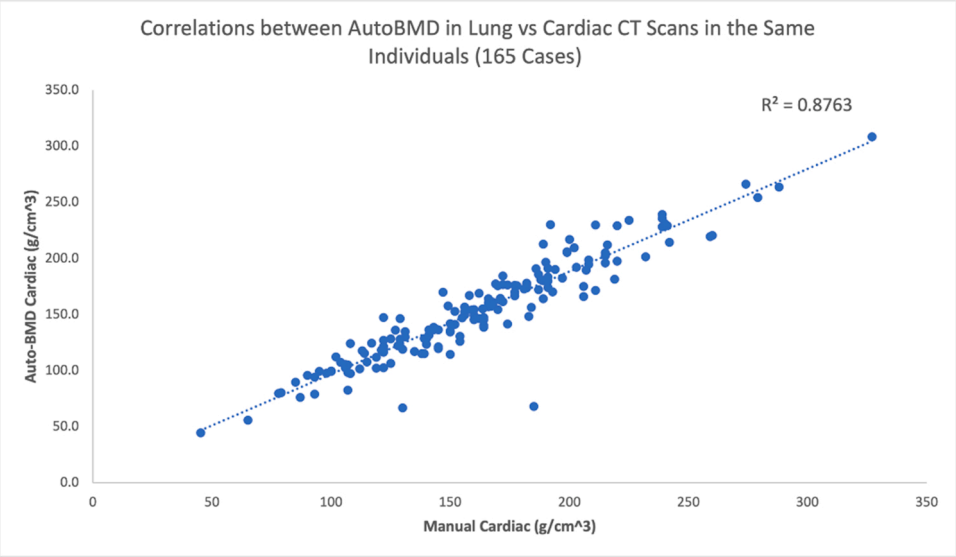

Fig. 5. Correlation of the average BMD obtained in 165 cases by the AutoBMD model for T7-T9 in lung and cardiac CT scans.

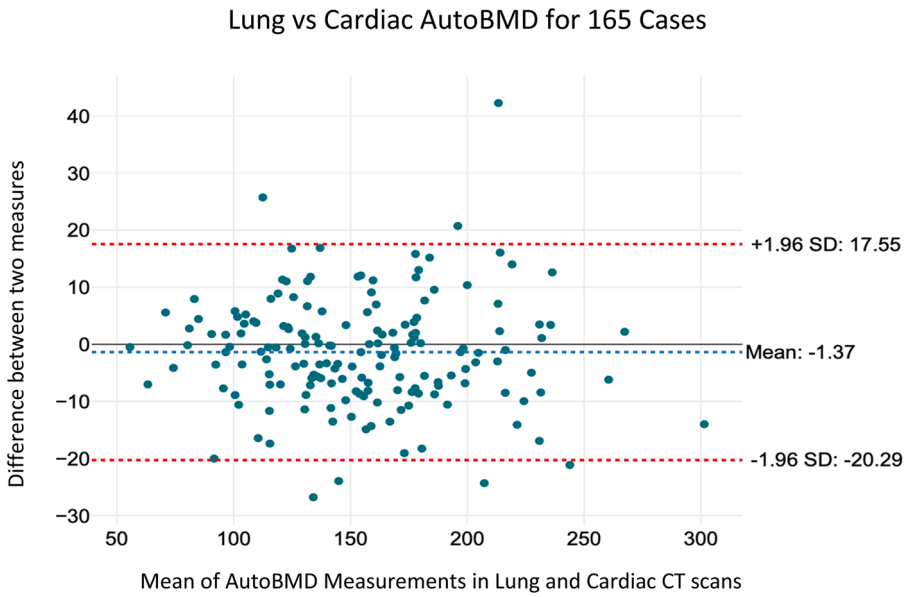

Fig. 6. Bland Altman plot for average BMD obtained by the Auto-BMD model for bones 7–9 for lung CT scans and bones 2–4 for cardiac CT scans.

Expenditures and funding sources

Funding for AutoBMD development was provided by American Heart Technologies LLC. Funding for qCT BMD measurements in coronary calcium scans were provided by NIH STTR grants 1R41AR070713–01 and 2R42AR070713–02A1.

Funding	Expenditure ($)
Budoff et al. STTR Phase 1 Contract: 1R41AR070713–01	**$149,165**
Budoff et al. STTR Phase 2 Contract: 2R42AR070713–02A1	**$996,254**

CRediT authorship contribution statement

Morteza Naghavi: Conceptualization, Methodology, Formal analysis, Funding acquisition, Investigation, Project administration, Supervision. **Isabel De Oliveira:** Formal analysis, Writing – original draft, Visualization. **Song Shou Mao:** Resources. **Amirhossein Jaberzadeh:** Software. **Juan Montoya:** Software. **Chenyu Zhang:** Software. **Kyle Atlas:** Formal analysis, Writing – review & editing, Visualization, Resources. **Venkat Manubolu:** Resources. **Marlon Montes:** Resources. **Dong Li:** Formal analysis, Data curation. **Thomas Atlas:** Formal analysis, Writing – review & editing, Visualization, Resources. **Anthony Reeves:** Resources, Investigation, Methodology, Writing - review & editing. **Claudia Henschke:** Resources, Investigation, Writing - review & editing. **David Yankelevitz:** Resources, Investigation, Writing - review & editing. **Matthew Budoff:** Investigation, Methodology, Resources, Writing - review & editing.

Declaration of Competing Interest

The authors declare the following financial interests/personal relationships which may be considered as potential competing interests: Morteza Naghavi reports financial support was provided by American

Technologies LLC and HeartLung.AI. Morteza Naghavi reports a relationship with American Technologies LLC and HeartLung.AI that includes: board membership, consulting or advisory, employment, and equity or stocks. Song Shou Mao reports a relationship with The Lundquist Institute that includes: consulting or advisory. Venkat Manubolu reports a relationship with HeartLung.AI that includes: consulting or advisory. Dong Li reports a relationship with HeartLung.AI that includes: consulting or advisory. Thomas Atlas reports a relationship with HeartLung.AI that includes: consulting or advisory. Anthony Reeves reports a relationship with HeartLung.AI that includes: consulting or advisory. Claudia Henschke reports no financial relationship with HeartLung.AI or American Heart Technologies LLC. David Yankelevitz reports a relationship with HeartLung.AI that includes: consulting or advisory. Matthew Budoff reports a relationship with HeartLung.AI that includes: consulting or advisory. Amirhossein Jaberzadeh reports a relationship with HeartLung.AI that includes: employment. Chenyu Zhang reports a relationship with HeartLung.AI that includes: employment. Marlon Montes reports a relationship with HeartLung.AI that includes: employment. Mathew Budoff has patent #US 9119,590 B2 issued to Los Angeles Biomedical Research Institute at Harbor-UCLA Medical Center, Torrance, CA. Mathew Budoff has patent #US 10,695,022,B2 issued to Los Angeles Biomedical Research Institute at Harbor-UCLA Medical Center, Torrance, CA.

References

[1] Y. Shen, X. Huang, J. Wu, et al., The global burden of osteoporosis, low bone mass, and its related fracture in 204 countries and territories, 1990-2019, Front Endocrinol. 13 (2022), 882241, https://doi.org/10.3389/fendo.2022.882241.

[2] M.A. Clynes, N.C. Harvey, E.M. Curtis, N.R. Fuggle, E.M. Dennison, C. Cooper, The epidemiology of osteoporosis, Br. Med. Bull. 133 (1) (2020) 105–117, https://doi.org/10.1093/bmb/ldaa005.

[3] US Preventive Services Task Force, S.J. Curry, A.H. Krist, D.K. Owens, M.J. Barry, A.B. Caughey, K.W. Davidson, C.A. Doubeni, J.W. Epling Jr, A.R. Kemper, M. Kubik, C.S. Landefeld, C.M. Mangione, M.G. Phipps, M. Pignone, M. Silverstein, M.A. Simon, C.W. Tseng, J.B. Wong, Screening for osteoporosis to prevent fractures: US preventive services task force recommendation statement, JAMA 319 (24) (2018) 2521–2531, https://doi.org/10.1001/jama.2018.7498.

[4] J.A. Kanis, H. Johansson, A. Odén, et al., Characteristics of recurrent fractures, Osteoporos. Int J. Establ Result Coop. Eur. Found. Osteoporos. Natl. Osteoporos. Found. USA 29 (8) (2018) 1747–1757, https://doi.org/10.1007/s00198-018-4502-0.

[5] K.N. Haseltine, T. Chukir, P.J. Smith, J.T. Jacob, J.P. Bilezikian, A. Farooki, Bone mineral density: clinical relevance and quantitative assessment, J. Nucl. Med Publ. Soc. Nucl. Med 62 (4) (2021) 446–454, https://doi.org/10.2967/jnumed.120.256180.

[6] ⟨https://www.bonehealthandosteoporosis.org/awareness-month/⟩. Bone Health & Osteoporosis Foundation. Accessed November 22, 2022.

[7] Aggarwal, C. Maslen, R.L. Abel, P. Bhattacharya, P.A. Bromiley, E.M. Clark, J. E. Compston, N. Crabtree, J.S. Gregory, E.P. Kariki, N.C. Harvey, K.A. Ward, K.E. S. Poole, Opportunistic diagnosis of osteoporosis, fragile bone strength and vertebral fractures from routine CT scans; a review of approved technology systems and pathways to implementation, 1759720×211024029–1759720×211024029, Ther. Adv. Musculoskelet. Dis. 13 (2021), https://doi.org/10.1177/1759720×211024029.

[8] M.K. Garg, S. Kharb, Dual energy X-ray absorptiometry: pitfalls in measurement and interpretation of bone mineral density, Indian J. Endocrinol. Metab. 17 (2) (2013) 203–210, https://doi.org/10.4103/2230-8210.109659.

[9] K.D. Harper, T.A. Clyburn, S.J. Incavo, B.S. Lambert, DEXA overestimates bone mineral density in adults with knee replacements, Sports Med Health Sci. 2 (4) (2020) 211–215, https://doi.org/10.1016/j.smhs.2020.10.002. PMID: 35782996; PMCID: PMC9219329.

[10] S.S. Mao, D. Li, Y.S. Syed, et al., Thoracic quantitative computed tomography (Qct) can sensitively monitor bone mineral metabolism: comparison of thoracic qct vs lumbar qct and dual-energy x-ray absorptiometry in detection of age-relative change in bone mineral density, Acad. Radio. 24 (12) (2017) 1582–1587, https://doi.org/10.1016/j.acra.2017.06.013.

[11] M.J. Budoff, Y.S. Hamirani, Y.L. Gao, et al., Measurement of thoracic bone mineral density with quantitative ct, Radiology 257 (2) (2010) 434–440, https://doi.org/10.1148/radiol.10100132.

[12] M.J. Budoff, J.M. Malpeso, I. Zeb, et al., Measurement of phantomless thoracic bone mineral density on coronary artery calcium CT scans acquired with various CT scanner models, Radiology 267 (3) (2013) 830–836, https://doi.org/10.1148/radiol.13111987.

[13] D. Li, S.S. Mao, B. Khazai, et al., Noncontrast cardiac computed tomography image-based vertebral bone mineral density: the Multi-Ethnic Study of Atherosclerosis (Mesa), Acad. Radio. 20 (5) (2013) 621–627, https://doi.org/10.1016/j.acra.2013.01.007.

[14] X.M. Xu, N. Li, K. Li, X.Y. Li, P. Zhang, Y.J. Xuan, X.G. Cheng, Discordance in diagnosis of osteoporosis by quantitative computed tomography and dual-energy X-ray absorptiometry in Chinese elderly men, J. Orthop. Transl. 18 (2018) 59–64, https://doi.org/10.1016/j.jot.2018.11.003. PMID: 31508308; PMCID: PMC6718941.

[15] W. Lin, C. He, F. Xie, T. Chen, G. Zheng, H. Yin, H. Chen, Z. Wang, Discordance in lumbar bone mineral density measurements by quantitative computed tomography and dual-energy X-ray absorptiometry in postmenopausal women: a prospective comparative study, Spine J. (2022) S1529–S9430 (22)01000-2.

[16] J.M. Weigert, QCT, the most accurate method of measuring bone mineral density? J. Bone Min. Res 12 (11) (1997) 1954–1955, https://doi.org/10.1359/jbmr.1997.12.11.1954.

[17] "Cardiovascular Diseases." World Health Organization, World Health Organization, ⟨https://www.who.int/health-topics/cardiovascular-diseases#tab=tab_1⟩.

[18] K. Inoue, T.E. Seeman, T. Horwich, M.J. Budoff, K.E. Watson, Heterogeneity in the Association between the presence of coronary artery calcium and cardiovascular events: a machine learning approach in the MESA study, Circ. Publ. Online (2022), https://doi.org/10.1161/CIRCULATIONAHA.122.062626.

[19] Schabath, B. Matthew, L. Michele, Cote, Cancer progress and priorities: lung cancer, Cancer Epidemiol., Biomark. Prev. vol. 28 (10) (2019) 1563–1579, https://doi.org/10.1158/1055-9965.epi-19-0221.

[20] Nupur Verma, et al., Lung cancer screening: how we do it and why, Semin. Roentgenol. vol. 55 (1) (2020) 14–22, https://doi.org/10.1053/j.ro.2019.10.004.

[21] Prema Nanavaty, et al., Lung cancer screening: advantages, controversies, and applications, Cancer Control vol. 21 (1) (2014) 9–14.

[22] L. Liu, M. Si, H. Ma, et al., A hierarchical opportunistic screening model for osteoporosis using machine learning applied to clinical data and CT images, BMC Bioinforma. 23 (1) (2022) 63, https://doi.org/10.1186/s12859-022-04596-z.

[23] L. Cherukuri, A. Kinninger, D. Birudaraju, et al., Effect of body mass index on bone mineral density is age-specific, Nutr. Metab. Cardiovasc Dis. NMCD 31 (6) (2021) 1767–1773, https://doi.org/10.1016/j.numecd.2021.02.027.

[24] S.S. Mao, D. Li, Y. Luo, Y.S. Syed, M.J. Budoff, Application of quantitative computed tomography for assessment of trabecular bone mineral density, microarchitecture and mechanical property, Clin. Imaging 40 (2) (2016) 330–338, https://doi.org/10.1016/j.clinimag.2015.09.016.

[25] L.D. Mesner, B. Ray, Y.H. Hsu, et al., Bicc1 is a genetic determinant of osteoblastogenesis and bone mineral density, J. Clin. Investig. 124 (6) (2014) 2736–2749, https://doi.org/10.1172/JCI73072.

[26] M.J. Budoff, W. Khairallah, D. Li, et al., Trabecular bone mineral density measurement using thoracic and lumbar quantitative computed tomography, Acad. Radio. 19 (2) (2012) 179–183, https://doi.org/10.1016/j.acra.2011.10.006.

[27] D. Massera, P. Buzkova, A.E. Bortnick, et al., Bone mineral density and long-term progression of aortic valve and mitral annular calcification: the multi-ethnic study of atherosclerosis, Atherosclerosis 335 (2021) 126–134, https://doi.org/10.1016/j.atherosclerosis.2021.08.031.

[28] Naghavi et al. Opportunistic Artificial Intelligence-based Detection of Osteoporosis and Osteopenia using Thoracic Vertebral Bone Mineral Density Measurements in Coronary Artery Calcium Scan. [In press, Journal of American College of Radiology].

[29] "Multi-Ethnic Study of Atherosclerosis." MESA, ⟨https://www.mesa-nhlbi.org/⟩.

[30] E.B. Gausden, B.U. Nwachukwu, J.J. Schreiber, D.G. Lorich, J.M. Lane, Opportunistic use of CT imaging for osteoporosis screening and bone density assessment: a qualitative systematic review, J. Bone Jt. Surg. Am. 99 (18) (2017) 1580–1590, https://doi.org/10.2106/JBJS.16.00749.

[31] Jiechao Ma, et al., Survey on deep learning for pulmonary medical imaging, Front. Med. vol. 14 (4) (2019) 450–469, https://doi.org/10.1007/s11684-019-0726-4.

[32] J.S. Chiu, Y.C. Li, F.C. Yu, Y.F. Wang, Applying an artificial neural network to predict osteoporosis in the elderly, Stud. Health Technol. Inf. 124 (2006) 609–614.

[33] Jiechao Ma, et al., Survey on deep learning for pulmonary medical imaging, Front. Med. vol. 14 (4) (2019) 450–469, https://doi.org/10.1007/s11684-019-0726-4.

[34] Y. Fang, W. Li, X. Chen, et al., Opportunistic osteoporosis screening in multi-detector CT images using deep convolutional neural networks, Eur. Radio. 31 (4) (2021) 1831–1842, https://doi.org/10.1007/s00330-020-07312-8.

[35] B. Cohen, N. Hiller, A. Szalat, V. Vainstein, OPPORTUNISTIC EVALUATION OF BONE MINERAL DENSITY BY PET-CT IN HODGKIN LYMPHOMA PATIENTS, Endocr. Pr. 25 (9) (2019) 869–876, https://doi.org/10.4158/EP-2019-0122. Epub 2019 Jun 6.

[36] K. Singer, S. Edmondston, R. Day, P. Breidahl, R. Price, Prediction of thoracic and lumbar vertebral body compressive strength: correlations with bone mineral density and vertebral region, Bone 17 (2) (1995) 167–174, https://doi.org/10.1016/s8756-3282(95)00165-4.

[37] J. Wendlová, Zmeny v denzite kostného minerálu v stavcoch Th12 az L5 pacientok s osteoporózou [Changes in bone mineral density in Th12 to L5 vertebrae in female patients with osteoporosis], Vnitr. Lek. 46 (8) (2000) 460–464. Slovak. PMID: 11048510.